

Microscopic Description of Exciton-Polaritons in Thin Semiconductor Layers

S. SCHUMACHER¹), G. CZYCHOLL, and F. JAHNKE

*Institute for Theoretical Physics, University of Bremen, P.O. Box 330 440, 28334 Bremen,
Germany*

(Received August 15, 2002; accepted August 22, 2002)

PACS: 71.35.Cc; 71.36.+c

Dedicated to Professor Dr. Roland Zimmermann on the occasion of his 60th birthday

Polariton effects in the optical spectra of thin semiconductor samples are analyzed within a microscopic theory based on a direct solution of the Schrödinger equation for the exciton motion in a finite sample. Various numerical schemes for the solution of the Schrödinger equation are discussed. Results are compared with the Pekar model augmented by phenomenologically introduced dead-layers at the surfaces. While the dead-layer is an unknown input parameter for macroscopic models based on additional boundary conditions, the microscopic theory can be used to determine the dead-layer thickness. Results are presented for various material systems. Furthermore the non-local excitonic susceptibility calculated within the microscopic theory in the frequency domain is presented.

1. Introduction Since the introduction of the polariton concept the interaction of a propagating light field with the excitonic polarization of bulk semiconductors or heterostructures has been the subject of intense experimental and theoretical research. Under realistic conditions, the presence of surfaces and the finite sample thickness can strongly modify excitonic properties due to the non-negligible spatial extension of the Coulomb bound electron–hole states. Near the surfaces, the semiconductor response function deviates strongly from that of the infinitely extended medium. The finite sample thickness leads to additional resonances in the optical spectra due to the interference of propagating polariton modes.

Our investigations are based on a microscopic theory [1, 2] where the excitonic polarization follows from a direct solution of the time dependent two-particle Schrödinger equation for the nonlocal excitonic transition amplitude of the spatially inhomogeneous system. Surface effects are included via microscopic boundary conditions for the excitonic transition amplitude. As an alternative approach to the scheme presented in Refs. [1] and [2] we start our calculations from an excitonic transition amplitude expressed in terms of the excitonic eigenstates calculated under microscopic boundary conditions. The propagating light field is directly computed from the Maxwell equations which are self consistently solved together with the inhomogeneous exciton equation. Our microscopic theory avoids so-called additional boundary conditions (ABC) which are necessary if one approximates the spatially nonhomogeneous and nonlocal excitonic polarization with that of the infinitely extended bulk material [3–5].

The confinement of excitons to a finite volume leads necessarily to a *nonlocal* optical susceptibility. In this contribution we analyze the nonlocal excitonic susceptibility for line-

¹) Corresponding author; e-mail: schumi@physik.uni-bremen.de

ar optical phenomena in a semiconductor layer by means of frequency-domain calculations including microscopic boundary conditions. The finite spatial extension of the exciton leads to polarization-free *dead-layers* near the surfaces. To improve the macroscopic models these dead-layers have been phenomenologically included as an additional parameter. However, our microscopic calculation shows that the dead-layer is different for various resonances of a single optical spectrum. As discussed below, this leads to clear deviations between the results of macroscopic models and microscopic calculations.

In Ref. [2] a situation has been analyzed where the experimentally observed transmission spectra of a high-quality 0.25 μm GaAs layer cannot be described in terms of ABC models. In this contribution we extend these investigations systematically to other material systems and determine the extension of the polarization free regions near the surfaces under various conditions from the microscopic theory.

2. Linear Light Propagation in Semiconductors When a light field propagates through a bulk semiconductor, a macroscopic polarization \mathbf{P} is induced which can be expressed in terms of the electron–hole transition amplitude ψ and the dipole matrix element \mathbf{d}_{cv} by

$$\mathbf{P}(\mathbf{r}, t) = \int d^3\rho \mathbf{d}_{cv}^* \psi(\mathbf{r}_e, \mathbf{r}_h, t), \tag{1}$$

where $\mathbf{r} = (\mathbf{r}_e + \mathbf{r}_h)/2$ and $\boldsymbol{\rho} = \mathbf{r}_e - \mathbf{r}_h$ are the sum and difference of the electron and hole coordinates, and the integration runs over the extension of the sample. For linear light propagation and in the effective-mass approximation the electron–hole transition amplitude obeys a two particle Schrödinger equation (inhomogenous exciton equation)

$$\left[i\hbar \frac{\partial}{\partial t} - E_g + \frac{\hbar^2}{2m_e^*} \nabla_e^2 + \frac{\hbar^2}{2m_h^*} \nabla_h^2 + V(\mathbf{r}_e - \mathbf{r}_h) \right] \psi(\mathbf{r}_e, \mathbf{r}_h, t) = -\mathbf{d}_{cv}(\boldsymbol{\rho}) \mathbf{E}(\mathbf{r}, t), \tag{2}$$

where V is the Coulomb interaction between electron and hole, E_g is the gap energy, $m_{e,h}^*$ are the effective electron and hole masses, and the driving term is due to the propagating electromagnetic field \mathbf{E} .

In this paper we consider a slab geometry (Fig. 1) where the electromagnetic field is a plane wave propagating in z -direction and the semiconductor sample is bounded by two surfaces perpendicular to the z -axis but extends homogeneously in the x - y -plane.

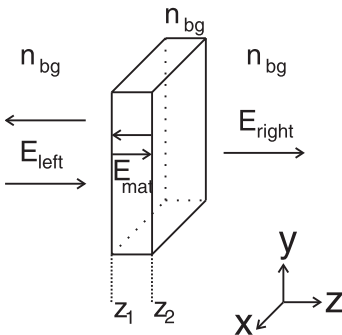


Fig. 1. Slab geometry. The electromagnetic field is propagating in z -direction and the semiconductor sample is bounded by two surfaces perpendicular to the z -axis but extends homogeneously in the x - y -plane

In the x - y -plane a separation of the electron-hole motion into relative and center-of-mass (COM) motion is still possible for each in-plane COM momentum \mathbf{q}_\perp ,

$$\psi_{\mathbf{q}_\perp}(\mathbf{r}_e, \mathbf{r}_h, t) = \psi(\mathbf{r}_{e\perp} - \mathbf{r}_{h\perp}, z_e, z_h, t) e^{i(\mathbf{q}_\perp \mathbf{R}_\perp - \omega_{\mathbf{q}_\perp} t)} = \psi(\mathbf{p}_\perp, z_e, z_h, t) e^{i(\mathbf{q}_\perp \mathbf{R}_\perp - \omega_{\mathbf{q}_\perp} t)}, \quad (3)$$

where \mathbf{p}_\perp and \mathbf{R}_\perp are the in-plane relative and COM coordinates, respectively. For the chosen geometry the in-plane COM momentum \mathbf{q}_\perp vanishes and only the $\mathbf{q}_\perp = 0$ part, denoted by $\psi(\mathbf{p}_\perp, z_e, z_h, t)$, contributes. Furthermore it is useful to Fourier transform the in-plane relative coordinates and to introduce the in-plane relative momentum \mathbf{k}_\perp according to

$$\psi(\mathbf{k}_\perp, z_e, z_h, t) = \int d^2\rho_\perp e^{i\mathbf{k}_\perp \rho_\perp} \psi(\mathbf{p}_\perp, z_e, z_h, t). \quad (4)$$

For rotational invariance around the direction of propagation ψ only depends on the modulus of the wave vector in the x - y -plane denoted by k_\perp , and the equation of motion for the electron-hole transition amplitude takes the form

$$\begin{aligned} i\hbar \frac{\partial}{\partial t} \psi(k_\perp, z_e, z_h, t) = & \left[E_g - i\gamma + \frac{\hbar^2 k_\perp^2}{2\mu^*} - \frac{\hbar^2}{2m_e^*} \frac{\partial^2}{\partial z_e^2} - \frac{\hbar^2}{2m_h^*} \frac{\partial^2}{\partial z_h^2} \right] \psi(k_\perp, z_e, z_h, t) \\ & - \int_0^\infty dk'_\perp k'_\perp V(k_\perp, k'_\perp, |z_e - z_h|) \psi(k'_\perp, z_e, z_h, t) \\ & - d_{cv} E(z, t) \delta(z_e - z_h). \end{aligned} \quad (5)$$

The Coulomb matrix elements

$$V(k_\perp, k'_\perp, |z_e - z_h|) = \frac{e^2}{8\pi^2 \varepsilon_0 n_{bg}^2} \int_0^{2\pi} d\phi_\perp \frac{e^{-|\mathbf{k}_\perp - \mathbf{k}'_\perp| |z_e - z_h|}}{|\mathbf{k}_\perp - \mathbf{k}'_\perp|}, \quad (6)$$

with $|\mathbf{k}_\perp - \mathbf{k}'_\perp| = \sqrt{k_\perp^2 + k'^2_\perp - 2k_\perp k'_\perp \cos \phi_\perp}$ contain the angle ϕ_\perp between \mathbf{k}_\perp and \mathbf{k}'_\perp , $n_{bg} = \sqrt{\varepsilon_{bg}}$ is the background refractive index, and γ is a phenomenological damping constant. We use the standard approximation of a momentum-independent dipole matrix element which corresponds to a delta-like space dependence in real-space formulation, $d_{cv}(z_e - z_h) = d_{cv} \delta(z_e - z_h)$.

The solution of Eq. (5) is uniquely determined by *microscopic boundary conditions*. For a finite sample the excitonic transition amplitude vanishes if either electron or hole reaches the medium's surface at z_1 or z_2

$$\begin{aligned} 0 = \psi(k_\perp, z_e = z_1, z_h, t) = \psi(k_\perp, z_e = z_2, z_h, t) = \psi(k_\perp, z_e, z_h = z_1, t) \\ = \psi(k_\perp, z_e, z_h = z_2, t). \end{aligned} \quad (7)$$

The evolution of the electromagnetic field is determined by the Maxwell equations which, for circularly polarized transverse fields propagating in z -direction, $\mathbf{E}(\mathbf{r}, t) = E(z, t) \mathbf{e}_+$ and $\mathbf{B}(\mathbf{r}, t) = B(z, t) i\mathbf{e}_+$ with $\mathbf{e}_+ = \frac{1}{\sqrt{2}} (\mathbf{e}_x + i\mathbf{e}_y)$, are

$$n_{bg}^2(z) \frac{\partial}{\partial t} E(z, t) = -c_0^2 \frac{\partial}{\partial z} B(z, t) - \frac{1}{\varepsilon_0} \frac{\partial}{\partial t} P(z, t), \quad (8)$$

$$\frac{\partial}{\partial t} B(z, t) = -\frac{\partial}{\partial z} E(z, t), \quad (9)$$

where $n(z)$ is the nonresonant (background) refractive index profile along the propagation direction. Within a homogeneous slab we have $n(z) = n_{bg}$. The source term in Eq. (8) couples the electromagnetic field to the macroscopic polarization $\mathbf{P}(\mathbf{r}, t) = P(z, t)\mathbf{e}_+$. The latter can be expressed in terms of the transition amplitude as

$$P(z, t) = \frac{1}{2\pi} \int_0^\infty dk_\perp k_\perp d_{cv}^* \psi(k_\perp, z, z, t) \quad (10)$$

with the help of Eqs. (1) and (4). In Eq. (10) we have again used a local dipole matrix element. Within the microscopic theory it is now possible to calculate the propagation of an electromagnetic light field through a thin semiconductor sample by selfconsistently solving the coupled set of Eqs. (5), (8–10). In the following we present a method to reduce the numerical effort for the calculation of the time evolution of Eq. (5).

The inhomogeneous exciton equation has the formal structure

$$i\hbar \frac{\partial}{\partial t} \psi(k_\perp, z_e, z_h, t) = \mathbf{H}\psi(k_\perp, z_e, z_h, t) - d_{cv}E(z, t) \delta(z_e - z_h), \quad (11)$$

where \mathbf{H} denotes the electron–hole Hamiltonian. We can expand the excitonic transition amplitude $\psi(k_\perp, z_e, z_h, t)$ into excitonic eigenstates $\psi_m(k_\perp, z_e, z_h)$ within the semiconductor slab under the boundary conditions (7) according to

$$\psi(k_\perp, z_e, z_h, t) = \sum_m a_m(t) \psi_m(k_\perp, z_e, z_h). \quad (12)$$

Inserting this expansion into the exciton Eq. (5) leads to

$$i\hbar \frac{\partial}{\partial t} \sum_m a_m(t) \psi_m(k_\perp, z_e, z_h) = \sum_m (\varepsilon_m - i\gamma) a_m(t) \psi_m(k_\perp, z_e, z_h) - d_{cv}E(z, t) \delta(z_e - z_h), \quad (13)$$

where ε_m are the eigenenergies corresponding to $\psi_m(k_\perp, z_e, z_h)$ and γ is a phenomenological damping constant. The orthonormality for the excitonic eigenstates $\psi_m(k_\perp, z_e, z_h)$ yields

$$i\hbar \frac{\partial}{\partial t} a_m(t) = (\varepsilon_m - i\gamma) a_m(t) - \frac{d_{cv}}{2\pi} \int_{z_1}^{z_2} dz E(z, t) \int_0^\infty dk_\perp k_\perp \psi_m^*(k_\perp, z, z). \quad (14)$$

To calculate the time evolution of the excitonic transition amplitude we have to solve an ordinary differential equation in time for each coefficient $a_m(t)$, where the driving terms are due to the projection of the electric field on the m^{th} eigenstate of the system. The macroscopic polarization (10) expressed in terms of eigenstates with time dependent coefficients is

$$P(z, t) = \frac{1}{2\pi} \sum_m a_m(t) \int_0^\infty dk_\perp k_\perp d_{cv}^* \psi_m(k_\perp, z, z). \quad (15)$$

Once we have calculated the excitonic eigenvalues and eigenstates for the slab geometry, it is only necessary to calculate the time evolution for the coefficients $a_m(t)$ to describe the behaviour of the medium coupled to an external electromagnetic field. The

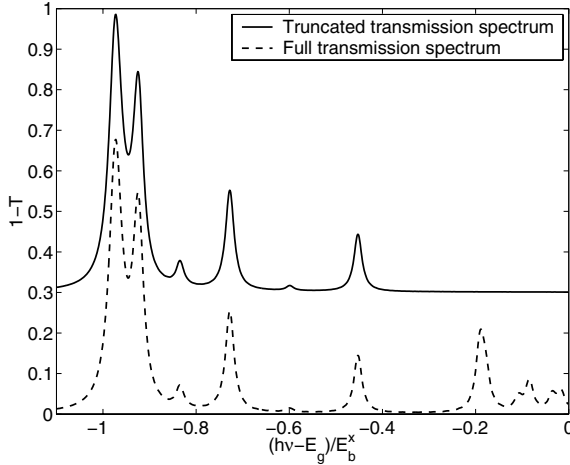


Fig. 2. Comparison of the transmission spectrum calculated by the full solution of the discretized Eq. (5) (dashed line) and the result of the microscopic theory where only seven excitonic eigenstates are taken into account (solid line; the $1-T$ -axis is shifted by 0.3 for these data because otherwise the two plots were almost indistinguishable from each other within a wide range of frequency). Results are shown for GaAs for a sample thickness $L = 10a_0^x$. The detuning is relative to the bulk semiconductor band gap energy E_g in units of the three-dimensional Rydberg energy E_b^x

Maxwell equations (8) and (9) can be solved as discussed in [2]. If we limit our calculations to the bound states of the system, it is sufficient to consider only the first few energetically lowest states. Within this approximation we are only left with a small number of ordinary differential equations for a finite number of coefficients $a_m(t)$. This approach nearly perfectly reproduces the results of the direct solution of Eq. (5) for the considered states if the corresponding eigenenergies are well separated from the neglected part of the spectrum. In Fig. 2 we show a comparison of a GaAs transmission spectrum obtained by a full solution of the discretized exciton Eq. (5) and a spectrum where only seven exciton eigenstates have been considered. For GaAs we use the following material parameters: $m_c^* = 0.067m_0$, $m_h^* = 0.457m_0$, $n_{bg} = 3.71$, $E_g = 1.42$ eV, $r_{cv} = 0.5$ nm, $\gamma = 0.04$ meV. Here n_{bg} is the background refractive index, γ is a damping constant, and r_{cv} is related to the dipole coupling constant $d_{cv} = er_{cv}$. The numerical effort of the eigenfunction expansion is reduced by more than one order of magnitude in comparison to the full solution.

3. A Closer Look at the ABC Problem In the last section we presented a theory to describe the propagation of electromagnetic fields through a semiconductor sample in the presence of boundaries which influence the exciton motion. In this approach the numerical complexity results from the coupling of the excitonic relative and COM motion. In the past, several approaches have been proposed based on an approximate decoupling of the excitonic relative and COM motion. However in the inhomogeneous case one cannot deduce independent boundary conditions for the relative and COM wave functions. For comparison with our full calculations we now outline briefly approximate treatments based on the dielectric theory of polaritons propagating in homogeneous media.

Taking into account only the interaction with the $1s$ -exciton resonance, one uses the two complex polariton wave vectors $q_{1,2}(\omega)$ describing the propagation of an optical field in the infinite system as an ansatz for the propagating electromagnetic field inside a finite semiconductor sample

$$E_{\text{mat}}(z, \omega) = \sum_{p=1,2} \left[E_p^+(\omega) e^{iq_p(\omega)z} + E_p^-(\omega) e^{-iq_p(\omega)z} \right]. \quad (16)$$

Here propagating and counter-propagating waves are considered for the slab geometry. Then the Maxwell boundary conditions are applied to connect the field inside the slab to free solutions of the Maxwell equations outside the sample. The simplest possible geometry involves an incident wave from the left and the reflected and transmitted components, E_r and E_t , with wave vectors $q_{\text{left}} = n_{\text{left}}\omega/c_0$ and $q_{\text{right}} = n_{\text{right}}\omega/c_0$,

$$E_{\text{left}}(z, \omega) = e^{iq_{\text{left}}z} + E_r(\omega) e^{-iq_{\text{left}}z}, \quad E_{\text{right}}(z, \omega) = E_t(\omega) e^{iq_{\text{right}}z}. \quad (17)$$

The continuity of E and $\partial E/\partial z$ on both boundaries determines only four of the six unknown coefficients $E_r(\omega)$, $E_t(\omega)$, $E_1^\pm(\omega)$, $E_2^\pm(\omega)$. The remaining two conditions are obtained by using additional boundary conditions (ABC) for the macroscopic polarization of the system. Pekar's ABC [3] require a vanishing macroscopic polarization at the sample surfaces,

$$P(\omega, z_1) = P(\omega, z_2) = 0. \quad (18)$$

For a discussion of other ABC, see [2, 5, 6]. With Eq. (18), the two remaining unknown coefficients can be uniquely determined from the macroscopic polarization, given by

$$P(\omega, z) = \sum_{p=1,2} \chi(q, \omega)|_{q=q_p(\omega)} \left[E_p^+(\omega) e^{iq_p(\omega)z} + E_p^-(\omega) e^{-iq_p(\omega)z} \right], \quad (19)$$

where $\chi(q, \omega)$ is the susceptibility of the infinitely extended bulk material.

4. Nonlocal Susceptibility In the previous section we presented an approximation using a local susceptibility $\chi(q, \omega)$ for the optical excitation of excitons which only depends on the COM momentum q of the exciton. In general the absence of translational symmetry in the z -direction for the discussed slab geometry results in a nonlocal susceptibility depending on two space coordinates. This susceptibility is defined by the formula for the macroscopic polarization induced by an electromagnetic field,

$$P(z, \omega) = \int dz' E(z', \omega) \chi(z, z', \omega). \quad (20)$$

The frequency dependent, nonlocal susceptibility can be calculated within the microscopic theory from the excitonic eigenstates $\psi_m(k_\perp, z_e, z_h)$ and the corresponding eigenenergies ε_m ,

$$\chi(z, z', \omega) = -\frac{|d_{cv}|^2}{(2\pi)^2} \sum_m \int dk_\perp dk'_\perp \frac{\psi_m^*(k'_\perp, z', z') \psi_m(k_\perp, z, z)}{\hbar\omega + i\gamma - \varepsilon_m}. \quad (21)$$

This result can be deduced from the general linear response theory, or by solving the inhomogeneous exciton equation in the frequency domain with the eigenfunction expansion of the excitonic transition amplitude. Figure 3 displays the space dependence of the imaginary (top) and real (bottom) part of the nonlocal susceptibility for the lowest three resonance peaks in Fig. 2. The imaginary part exhibits standing wave like structures due to the boundary conditions (7) at the surfaces of the semiconductor slab. In a simplified picture these structures can be interpreted as a quantization of the exciton COM motion. In the following we will have a closer look at the validity of such a simplified model where the exciton is treated as a point-like particle without spatial extension.

Using the nonlocal susceptibility (21) an alternative way for the calculation of optical spectra is the selfconsistent solution of the inhomogeneous wave equation for the

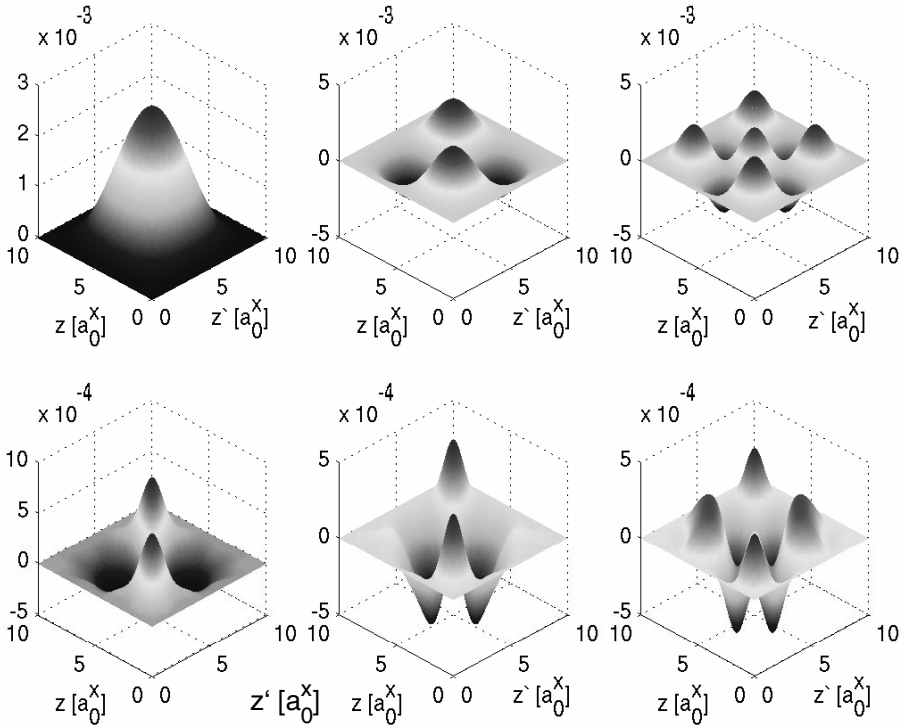


Fig. 3. Nonlocal susceptibility for the lowest three resonance frequencies in Fig. 2, increasing frequency from left to right. Top: imaginary part, bottom: real part

electric field

$$\left[\frac{\partial^2}{\partial z^2} + n_{\text{bg}} \frac{\omega^2}{c_0^2} \right] E(z, \omega) = - \frac{\omega^2}{\epsilon_0 c_0^2} \int dz' \chi(z, z', \omega) E(z', \omega) \quad (22)$$

in frequency domain, leading to the same results as the time-dependent calculations presented in the first section.

5. Introduction of the Dead-Layer Concept The solid line in Fig. 4 shows the calculated transmission spectrum of a GaAs sample with a thickness of 125 nm which is equivalent to $10a_0^X$ where a_0^X is the exciton Bohr radius. The corresponding space dependence of the macroscopic polarization for various frequency components of the spectrum can be obtained from a solution of the microscopic theory for stationary, monochromatic excitation of the sample. For excitation frequencies corresponding to the resonances in Fig. 4 (solid line), which are consecutively labeled by n , results are given in Fig. 5.

The polarization exhibits standing-wave like states within the slab which corresponds to the naive picture of a COM quantization of the exciton movement in z -direction, but with an effectively decreased sample thickness. Obviously, the system contains surface layers with negligible macroscopic polarization of the semiconductor

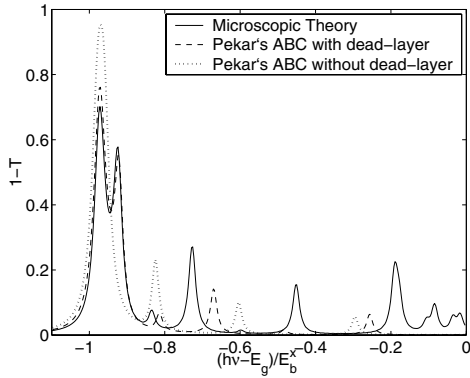


Fig. 4

Fig. 4. Calculated GaAs transmission spectrum for a sample thickness $L = 10a_0^x$. The detuning is relative to the bulk semiconductor band gap energy E_g in units of the three-dimensional Rydberg energy E_b^x

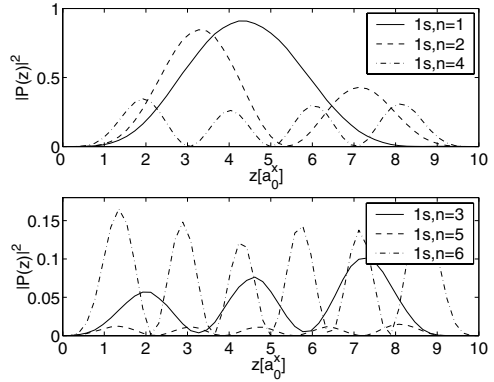


Fig. 5

Fig. 5. Spatial distribution of the macroscopic polarization for stationary, monochromatic excitation. The excitation frequency is tuned to the resonances of the system (solid line in Fig. 4)

due to the finite spatial extension of the exciton as a Coulomb bound state of electron and hole. The situation is further complicated by the fact that the thickness of these layers differs for various resonance frequencies.

When Pekar's ABC are used to calculate optical spectra, the boundary conditions are only imposed on the COM motion within the slab, leading to discrete energies $E_n = E_b^x + \frac{\hbar^2 \pi^2 n^2}{2M^* L^2}$. The corresponding transmission spectrum is shown as a dotted line in Fig. 4. To include the finite spatial extension of the excitonic states in this picture in an approximative way one additionally assumes dead-layers of length d at the surfaces of the sample. Using the results of the microscopic theory displayed in Fig. 4, we estimate for the $n = 1$ resonance an effective sample thickness $L_{\text{eff}} = L - 2d = 7.2a_0^x$.

The result of a calculation with Pekar's ABC using the dead-layer determined for the first resonance $n = 1$ is shown as dashed line in Fig. 4. The structure of the double-peak main resonance is nearly reproduced, but the energetic positions of the excitonic higher replicas are shifted to higher energies in comparison to the microscopic spectrum, since the higher polariton modes show much smaller dead-layers than the main resonance, see Fig. 5.

6. Various Material Systems

To extend the results discussed above to other material systems, we show in Figs. 6 and 7 calculated transmission spectra for CdTe and ZnSe, respectively. We chose again sample thicknesses of $10a_0^x$ for the calculations corresponding to 66 nm for the heavy-hole exciton in CdTe and to 34 nm for the heavy-hole exciton in ZnSe. The microscopic calculations are compared to Pekar's ABC, where for the latter the dead-layer was chosen to best fit the main resonances of the microscopic spectra. For the calculations the following material parameters were used: $m_e^* = 0.087m_0$, $m_{\text{hh}}^* = 0.601m_0$, $n_{\text{bg}} = 3.11$, $E_g = 1.595$ eV, $r_{\text{cv}} = 0.43$ nm, $\gamma = 0.12$ meV, (CdTe), $m_e^* = 0.16m_0$, $m_{\text{hh}}^* = 0.78m_0$, $n_{\text{bg}} = 2.95$, $E_g = 2.85$ eV, $r_{\text{cv}} = 0.15$ nm,

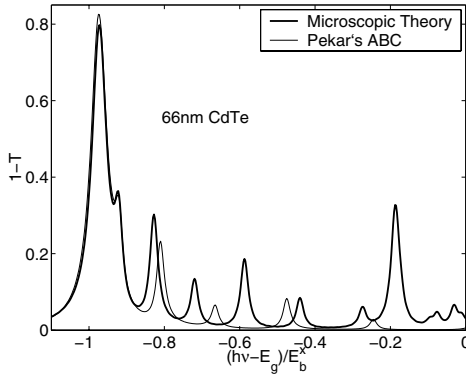


Fig. 6

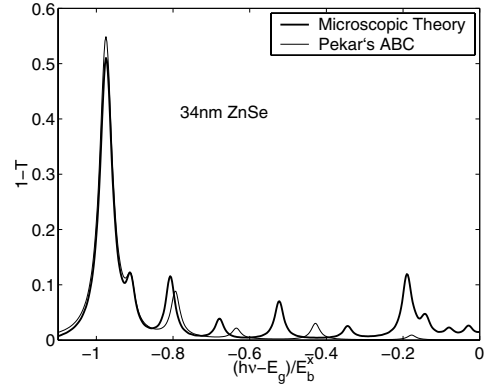


Fig. 7

Fig. 6. Calculated CdTe (heavy-hole) transmission spectrum for a sample thickness $L = 10a_0^x$ corresponding to 66 nm. Microscopic theory (thick line) and Pekar's ABC with appropriate dead-layer (thin line)

Fig. 7. Calculated ZnSe (heavy-hole) transmission spectrum for a sample thickness $L = 10a_0^x$ corresponding to 34 nm. Microscopic theory (thick line) and Pekar's ABC with appropriate dead-layer (thin line)

$\gamma = 0.32$ meV, (ZnSe). We find a similar behaviour as in the GaAs material system. The first two resonances of the microscopic calculation can be fitted within the ABC model with properly chosen dead-layer. Then, however, the energetic position as well as the height of the higher resonances are not well reproduced.

7. Dependence of the Dead-Layer on the Reduced Exciton Mass Having introduced the dead-layer as a phenomenological parameter for augmenting Pekar's ABC, we would like to use the microscopic model to systematically determine the influence of material parameters and excitation frequency on the dead-layer thickness. The motion of electron and hole relative to the excitonic COM coordinate is characterized by the reduced exciton mass μ^* normalized to the total exciton mass M^* , as it is already clear from the naive picture of electron and hole treated as rigid balls, see Fig. 8. If the electron and hole masses are approximately the same, the COM is in the center between electron and hole, and as the electron–hole transition amplitude must vanish at the surface, the COM can approach the surface up to half an exciton Bohr radius. If the hole is much heavier than the electron, the COM is approximately at the hole position, and as the electron–hole transition amplitude must vanish at the surface, the COM distance to the surface would be at least one exciton Bohr radius.

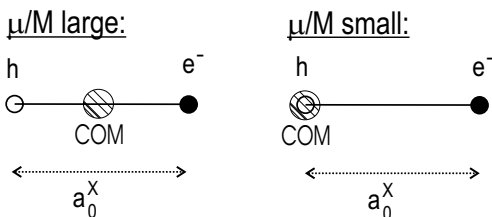


Fig. 8. Illustration of the rigid ball model for the exciton. The two limiting cases are displayed, equal electron and hole masses and infinitely heavy hole. A detailed discussion is given in the text

For a general discussion of this behaviour we investigate the dependence of the dead-layer thickness on the reduced exciton mass normalized to the total exciton mass μ^*/M^* . The limiting cases of equal electron–hole masses and infinitely heavy holes correspond to $\mu^*/M^* = 1/4$ and $\mu^*/M^* = 0$, respectively. Recent investigations of the dead-layer in [7] have been based on an approximate decoupling of the exciton relative and COM motion by using a Born–Oppenheimer procedure for the excitonic ground state. Furthermore, different dead-layers for various resonances have not been considered. In the following, we use the microscopic model calculations (without the necessity to approximately decouple relative and COM motion) to extract the dead-layer, also including polaritonic effects.

For layer thicknesses of $10a_0^x$ several transmission spectra for various reduced exciton masses are calculated. Since the determined dead-layer will be used to augment Pekar’s ABC, the determination process is as follows: By varying the dead-layer thickness (which corresponds to a variation of the effective layer thickness) we fit the position of the considered resonance of the Pekar spectrum to the corresponding peak in the spectrum of the microscopic calculation. Note that the procedure is only meaningful as long as the influence of the quantum confinement on the electron–hole relative motion is not too strong. Otherwise the dead-layer concept fails.

Our calculations quantitatively reproduce the results published in [7] for the excitonic ground state in a slab geometry, see results for the lowest peak ($n = 1$) in Fig. 9. Furthermore, we observe the expected growth of the dead-layer with decreasing reduced exciton masses, as predicted from the simple rigid-ball model. For equal electron and hole masses ($\mu^*/M^* = 0.25$) one nearly obtains the expected value of $0.5a_0^x$ for the dead-layer, but it increases faster for decreasing μ^*/M^* than the naive rigid-ball picture can explain.

Additionally there is a variation of the dead-layer for the different resonance peaks in each spectrum which is more important for decreasing μ^*/M^* . For $\mu^*/M^* \approx 0.11$, as it was used for GaAs examples, we see that different dead-layers have to be chosen for the different resonances. From this point of view it is clear why a constant dead-layer which well fits the main resonance shifts the higher polariton-states to higher energies in comparison to the microscopic theory. These theoretical considerations show, that

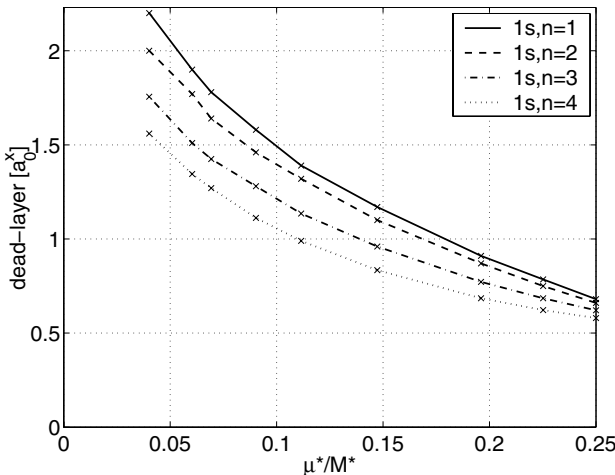


Fig. 9. Dead-layer dependence on the reduced exciton mass μ^* normalized to the total exciton mass M^* for a sample thickness of $10a_0^x$ (exciton Bohr radius). The dead-layer is given in units of the exciton Bohr radius a_0^x for each μ^*/M^*

there is no justification for the assumption of a constant dead-layer to reproduce a whole spectrum of bound exciton-states with Pekar's ABC.

8. Conclusion Linear transmission spectra for thin GaAs, CdTe, and ZnSe samples have been discussed. Different methods for the solution of the microscopic model have been presented all leading to the same results. The calculated transmission spectra have been compared to the results obtained by Pekar's ABC with dead-layers at the surfaces. Furthermore the dependence of the dead-layer on the reduced exciton mass and on the excitation frequency has been evaluated. A detailed comparison of experimentally obtained transmission spectra from ZnSe samples of several thicknesses to the full microscopic calculation and to Pekar's ABC is currently in progress.

Acknowledgements F. J. acknowledges a grant for CPU time from the John von Neumann Institute for Computing at the Forschungszentrum Jülich.

References

- [1] J. TIGNON, T. HASCHE, D. S. CHEMLA, H. C. SCHNEIDER, F. JAHNKE, and S. W. KOCH, *Phys. Rev. Lett.* **84**, 3382 (2000).
- [2] H. C. SCHNEIDER, F. JAHNKE, S. W. KOCH, J. TIGNON, T. HASCHE, and D. S. CHEMLA, *Phys. Rev. B* **63**, 045202 (2001).
- [3] S. I. PEKAR, *Sov. Phys. JETP* **6**, 785 (1958).
- [4] J. J. HOPFIELD, *Phys. Rev.* **112**, 1555 (1958).
- [5] C. S. TING, M. J. FRANKEL, and J. L. BIRMAN, *Solid State Commun.* **17**, 1285 (1975).
- [6] K. HENNEBERGER, *Phys. Rev. Lett.* **80**, 2889 (1998).
- [7] M. COMBESCOT, R. COMBESCOT, and B. ROULET, *Eur. Phys. J. B* **23**, 139 (2001).